Absorption of waves by large-scale winds in stratified turbulence

P. Clark di Leoni and P. D. Mininni
Departamento de Física, Facultad de Ciencias Exactas y Naturales, Universidad de Buenos Aires and IFIBA, CONICET, Ciudad Universitaria, 1428 Buenos Aires, Argentina

(Received 4 August 2014; revised manuscript received 20 January 2015; published 26 March 2015)

The atmosphere is a nonlinear stratified fluid in which internal gravity waves are present. These waves interact with the flow, resulting in wave turbulence that displays important differences with the turbulence observed in isotropic and homogeneous flows. We study numerically the role of these waves and their interaction with the large-scale flow, consisting of vertically sheared horizontal winds. We calculate their space- and time-resolved energy spectrum (a four-dimensional spectrum) and show that most of the energy is concentrated along a dispersion relation that is Doppler shifted by the horizontal winds. We also observe that when uniform winds are let to develop in each horizontal layer of the flow, waves whose phase velocity is equal to the horizontal wind speed have negligible energy. This indicates a nonlocal transfer of their energy to the mean flow. Both phenomena, the Doppler shift and the absorption of waves traveling with the wind speed, are not accounted for in current theories of stratified wave turbulence.

DOI: 10.1103/PhysRevE.91.033015 PACS number(s): 47.27.ek, 47.35.Bb

I. INTRODUCTION

Turbulent flows are often pictured as highly disorganized, with energy being transferred from large-scale motions to small-scale eddies. But in some cases the opposite can happen. In 1967 Kraichnan [1] developed the theory of the inverse energy cascade, in which nonlinearities transfer energy towards larger structures in a self-organization process. The theory had a huge impact in oceanography and meteorology and in the basic physical understanding of turbulence. However, an inverse cascade is not the only possible mechanism by which energy can be transferred from small to large scales, and in some flows other mechanisms can result in the generation of large-scale flows.

An important example is given by stratified flows. Stratification plays a key role in the dynamics of the oceans and the atmosphere. As an example, internal gravity waves arising from it are responsible for transfer of momentum between different regions of the atmosphere [2] and for transport in the oceans [3,4]. Much effort has been put into characterizing internal gravity waves and their relation with geophysical flows [5–7].

Several observational studies suggest there is a coupling between the mean (or large-scale) flow and internal gravity waves [8–10]. As a result, various models for the interaction between a wave field and a mean background flow have been put forward [11–13]. These models, which were mainly developed in the context of atmospheric sciences and oceanography, predict that the dispersion relation of the waves is Doppler shifted by the background flow. Furthermore, they also describe a mechanism by which waves whose horizontal phase velocity matches that of the horizontal wind speed on a given layer of the fluid, are absorbed by the background flow. The layer where this happens is the so-called critical layer (CL). The absorption of the waves can be viscous or the result of an instability, with one or the other mechanism being dominant depending on the parameters of the system. The wave energy can then be absorbed and dissipated, or a fraction can be re-emitted or transferred towards the mean flow.

Critical layers are also relevant in Rossby wave turbulence in geophysical flows and in wave-flow interactions in plasmas [14–16]. However, most CL models are either linear or perturbative, have the large-scale shear externally imposed, lack nonlinear coupling between the waves themselves as well as with small-scale eddies, and cannot fully describe the nonlinear dynamics of a turbulent geophysical flow. Important observational studies of the atmosphere [17] and the ocean [18], and laboratory experiments [19,20] focusing on the properties of single waves passing through, show Doppler shift and indications of absorption in the CL, although they lack the presence of a fully developed turbulent superposition of waves. In the same spirit, numerical studies of Doppler shift and CL absorption [12,13,21,22] that solve nonlinear atmospheric models focus on single wave packets interacting with a background flow which is externally imposed and do not take into account the turbulent nature of geophysical flows nor the nonlinear interaction between the internal gravity waves themselves and with the eddies present in the flow (see, however, Ref. [21], where the full nonlinear equations are solved, although a single wave-packet and background flow are imposed). This can be understood as identifying waves in a smooth flow can be done by observing the time evolution of the system, while extraction of the waves in a disordered background requires space and time information.

On the other hand, fluid dynamics studies, both theoretically and numerically (see, e.g., Refs. [23–26]), focused mainly on the fully nonlinear aspect of stratified turbulence, on how energy is distributed among scales, and on the development of anisotropy and of flat "pancake" structures in the flow. These studies remark that the interaction between waves and eddies is of fundamental importance in stratified turbulence but have neglected the effects of Doppler shifts or CL absorption. An important topic which is subject to an active debate is the existence of an inverse cascade in purely stratified flows. As already mentioned, an inverse cascade is a self-similar process by which energy is transferred nonlinearly from small scales to larger scales, so energy gets accumulated in structures with larger correlation length than that of the

injection mechanism. Inverse cascades have been extensively studied in two-dimensional turbulence [1] and have also been observed in rotating turbulence (including rotating stratified turbulence) [27–29]. But results for purely stratified turbulence are unclear. It is known that stratified flows can generate large-scale vertically sheared horizontal winds (VSHW) [30], although the mechanism involved is not entirely understood. While evidence of energy flow toward large scales has been reported [31,32], several authors have argued that an inverse cascade is not possible [24,33] based on statistical mechanical arguments.

Recently, weak turbulence theory [34,35] has also been used to study stratified turbulence, although only considering the coupling between the waves and not with the eddies. While this theory can give information on the formation of the nonlinear energy cascade, it cannot characterize interactions of the wave field with a mean flow. Some extensions that consider nonlocal interactions and the development of zonal flows have been proposed to address this and are specially relevant in the context of quasigeostrophic turbulence [36] and plasma turbulence in tokamaks [37,38] to explain the development of large-scale flows.

In this article, we identify a mechanism working within a stably stratified turbulent flow that couples the wave field with the large-scale VSHW, thus gaining a better understanding of the role of waves and the generation of large structures in turbulent flows. We obtain four-dimensional space- and time-resolved energy spectra, allowing us to uniquely identify the wave components of the total flow and to study their dynamics. We show that waves are Doppler shifted by the VSHW and that while a direct nonlinear energy cascade is present, energy can also be transferred nonlocally from the small-scale waves to the large-scale flow though absorption in the CL. Finally, we also show that the energy spread created by the Doppler shift is not uniform, a fact that results from the turbulent nature of the dynamically evolving large-scale flow.

II. STABLY STRATIFIED FLOWS

In this section we present the equations we solve numerically that describe a stably stratified flow, introduce characteristic time scales, and give a brief introduction to the linear theory of gravity waves in the presence of background shear.

A. The Boussinesq equations

We consider the Boussinesq equations describing an incompressible stratified flow,

$$\partial_t \mathbf{u} + \mathbf{u}\cdot\nabla\mathbf{u} = -\nabla p - N\theta\hat{z} + \nu\nabla^2\mathbf{u} + \mathbf{F}, \tag{1}$$

$$\partial_t \theta + \mathbf{u}\cdot\nabla\theta = N u_z + \kappa\nabla^2\theta, \tag{2}$$

where $\mathbf{u}$ is the velocity field (with $\nabla\cdot\mathbf{u}=0$), θ is the potential temperature fluctuations, p is the pressure normalized by the mean fluid density, ν is the kinematic viscosity, κ is the thermal diffusivity, N is the Brunt-Väisälä frequency (associated with the vertical background stratification), and $\mathbf{F}$ is an external mechanical forcing.

In the absence of a background flow, of forcing ($\mathbf{F}=0$), and of viscosity and diffusion ($\nu=\kappa=0$), Eqs. (1) and (2) have as exact nonlinear solutions [39] internal gravity waves with the dispersion relation

$$\omega_0 = N\frac{k_\perp}{k}. \tag{3}$$

Here $k_\perp = (k_x^2+k_y^2)^{1/2}$ is the wave number perpendicular to gravity. Gravity acts along the $\hat{z}$ axis, with associated wave number $k_\parallel = k_z$ such that $k=(k_\perp^2+k_\parallel^2)^{1/2}$.

B. Characteristic time scales

The important characteristic time scales that come into play in this system are the wave period τ_ω and the nonlinear turnover time $\tau_{\rm NL}$. The wave period is simply given by $\tau_\omega \propto 1/\omega_0$. The nonlinear turnover time is the time taken by an eddy at a certain scale to transfer its energy through nonlinear interactions to smaller-scale eddies locally in wave-number space. From dimensional analysis, this time scale can be estimated as

$$\tau_{\rm NL} \propto \frac{\ell}{u_\ell} \propto \frac{1}{k\sqrt{kE(k)}}, \tag{4}$$

where $\ell \propto 1/k$ is a length scale in the inertial range, u_ℓ is the characteristic velocity of eddies at scale ℓ, and $E(k)$ is the energy spectrum. If the energy spectrum in stratified turbulence follows a power law $E(k)\propto k^{-3}$ (see, e.g., Ref. [23]), then it is easy to show that the turnover time is independent of the scale and becomes $\tau_{\rm NL}\propto L/u_{\rm rms}$ at all scales.

C. Gravity waves in a background flow

In the presence of a background horizontal flow $\mathbf{U}(z)$, the frequency measured by an observer is shifted by the Doppler effect, resulting in a frequency

$$\omega = \omega_0 + \mathbf{U}\cdot\mathbf{k}_\perp. \tag{5}$$

Considering for simplicity the unidirectional case with $\mathbf{U}=U(z)\hat{x}$ and substituting

$$\mathbf{u} = \mathbf{U} + \mathbf{u}' \tag{6}$$

in Eqs. (1) and (2) with $\mathbf{u}' = w(z)e^{ik_\perp(x-ct)}\hat{z}$ a planar internal gravity wave propagating in $\hat{x}$ with phase velocity $c=\omega/k$, we obtain after linearization an equation for the vertical velocity amplitude [40],

$$\frac{\partial^2 w}{\partial z^2} + \left[\frac{N^2}{(U-c)^2} - \frac{d^2U/dz^2}{U-c} - k_\perp^2\right] w = 0. \tag{7}$$

This equation has a singularity when $c=U(z)$, which is associated with the existence of a CL in which the Reynolds stress tensor has a discontinuity [40]. As a result, a wave traveling through the fluid an approaching the layer with $c=U(z)$ develops faster and faster fluctuations. In nature, the eventual development of a singularity is arrested either by viscous damping [12,41,42] or by nonlinearities [43–45]. In the former case dissipation regularizes the solution as the wave approaches the CL, preventing the amplitude of the wave from going to infinity while absorbing its energy. In the latter, the solution becomes unstable and finally degenerates into turbulence, transferring a fraction of its energy to the

background flow. These latter processes cannot be properly described by the linear theory. Note that the CL mechanism can only occur if the Richardson number based on the background flow, $\mathrm{Ri}^{\mathrm{BF}} = N^2/(\partial_z U)^2$, is greater than 1/4 [12,40].

An interesting numerical study beyond the linear regime presented in Ref. [21] considers the energy balance when a wave packet crosses a CL. The authors were able to quantify that more than a third of the energy in the waves is nonlocally transferred to the mean background flow, while the rest of the energy in the waves is transferred towards the small-scale turbulence where it is finally dissipated.

III. NUMERICAL SIMULATIONS

Direct numerical simulations of Eqs. (1) and (2) were performed in a cubic periodic box using the parallel code GHOST [46–48] that uses a pseudospectral method to estimate spatial derivatives and evolves the system in time using a second-order Runge-Kutta method. Two forcing functions were used: Taylor-Green forcing with $\mathbf{F} = f_0(\sin x \cos y \cos z\, \hat{x} - \cos x \sin y \cos\, \hat{z})$ and a randomly generated three-dimensional forcing acting at $k = 1$ (a third set of simulations, with a different forcing scheme, is presented in the Appendix). As we will consider frequency spectra, in all cases the forcing was kept constant in time to prevent exciting spurious time scales in the system and to prevent disrupting the development of VSHW.

A Taylor-Green flow excites two-dimensional motions and has been used in previous studies of stably stratified turbulence to mimic atmospheric motions [49], while three-dimensional forcing injects energy directly into vertical motions and thus excites stronger gravity waves. Some of the effects we show are disrupted when VSHW cannot fully develop, so in the next section we focus first on the three-dimensional forcing case with strong stratification. Then, in Sec. IV C, we present results comparing both forcings and explain in more detail the impact of Taylor-Green forcing in the development of CLs. In that section, we also analyze the effects of varying the level of stratification.

The simulations can be characterized with dimensionless numbers. All simulations have Reynolds number $\mathrm{Re} = Lu_{\mathrm{rms}}/\nu \approx 9700$ (where L is the forcing scale and u_{rms} is the r.m.s. velocity of order unity) and Prandtl number $\mathrm{Pr} = \nu/\kappa = 1$. For each forcing function, we performed three simulations with varying stratification N, resulting in Froude numbers $\mathrm{Fr} = u_{\mathrm{rms}}/(NL) \approx 0.04$, 0.02, and 0.01 (with decreasing Fr indicating stronger stratification) and buoyancy Reynolds number $\mathrm{Re_b} = \mathrm{ReFr}^2 \approx 15$, 3.9, and 0.97. Each simulation was started from the fluid at rest, so neither the large-scale flow nor the small-scale waves were previously imposed, and the simulations were continued for 12 large-scale turnover times to let the system reach a turbulent steady state. Then each simulation was continued for other 12 turnover times saving all fields with high temporal cadence, resulting in 1200 outputs of each field that sample the Brunt-Väisälä frequency 40 times per period when $\mathrm{Fr} \approx 0.01$. This previously unmatched temporal resolution allows us to resolve four-dimensional spectra simultaneously in space and in time, although at a computational cost that allows us to reach only moderate spatial resolutions with 512^3 spatial grid points. Nonetheless, as we show, the spatial resolution we use is appropriate, and recent studies also indicate that properties of fully developed turbulence can be identified even at moderate resolutions [50].

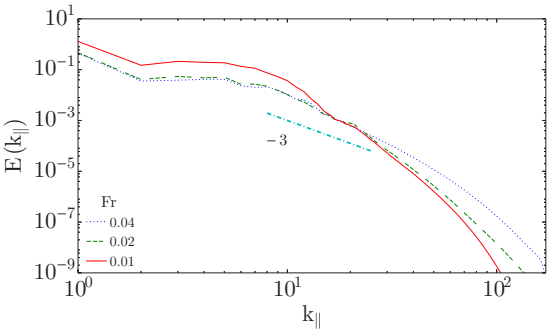

FIG. 1. (Color online) Reduced parallel energy spectrum $E(k_\parallel)$ for the three simulations with three-dimensional forcing. A $k_\parallel^{-3}$ slope is shown only as a reference.

IV. RESULTS

A. Spatial spectral analysis

Traditional characterization of turbulent flows is done using one-dimensional spectra. In Fig. 1 we present the parallel spectrum $E(k_\parallel)$ for the three simulations with three-dimensional forcing. Only as a reference, we also show in Fig. 1 a power law $\propto k_\parallel^{-3}$. The reader can find detailed spatial characterizations of stratified turbulence, which go beyond the aim of this work and at higher spatial resolution in recent studies (see, e.g., Refs. [24,25]).

As a better way to characterize energy distribution among scales in the presence of anisotropy, Fig. 2 shows the spatial axisymmetric energy spectrum $e(k_\perp, k_\parallel)$, normalized by $\sin\theta$ with $\theta = \arctan(k_\perp/k_\parallel)$ to obtain circular isocontours in the case of an isotropic flow. In Fig. 2, two spectra are presented for the simulations with three-dimensional forcing and $\mathrm{Fr} \approx 0.02$ and $\approx$0.01. As stratification is increased, energy distribution becomes more anisotropic, with energy being preferentially transferred towards modes with smaller $k_\perp$ (and, as a result, larger wave period) [23–25,30]. However, for $\mathrm{Fr} \approx 0.01$ energy accumulates near the modes with wave period ($\tau_\omega \propto 1/\omega_0$) equal to the nonlinear turnover time ($\tau_{\mathrm{NL}} \propto L/u_{\mathrm{rms}}$), forming a ridge. As the energy transfer mechanism is often given by the shortest time scale [51], modes below the curve $\tau_\omega = \tau_{\mathrm{NL}}$ (those with wave period shorter than the turnover time) are associated with waves [24,25,30]. Modes above the curve $\tau_\omega = \tau_{\mathrm{NL}}$ (and, in particular, modes with $k_\perp = 0$) are often called vortical modes, as for these modes $\omega_0 \approx 0$. The fraction of the energy in these modes decreases with decreasing Fr, in good agreement with the observed accumulation near $\tau_\omega = \tau_{\mathrm{NL}}$ for large Fr. The slowdown of the transfer as the energy reaches the ridge is compatible with critical balance arguments [34] and is also of great importance in weak wave turbulence theories [35] that require the energy of the system to remain in weakly interacting waves. Note, however, that this distinction between waves and vortical modes in Fig. 2, based on the characteristic time of each mode, is only approximate. A strict discrimination between waves and eddies requires the four-dimensional spectrum.

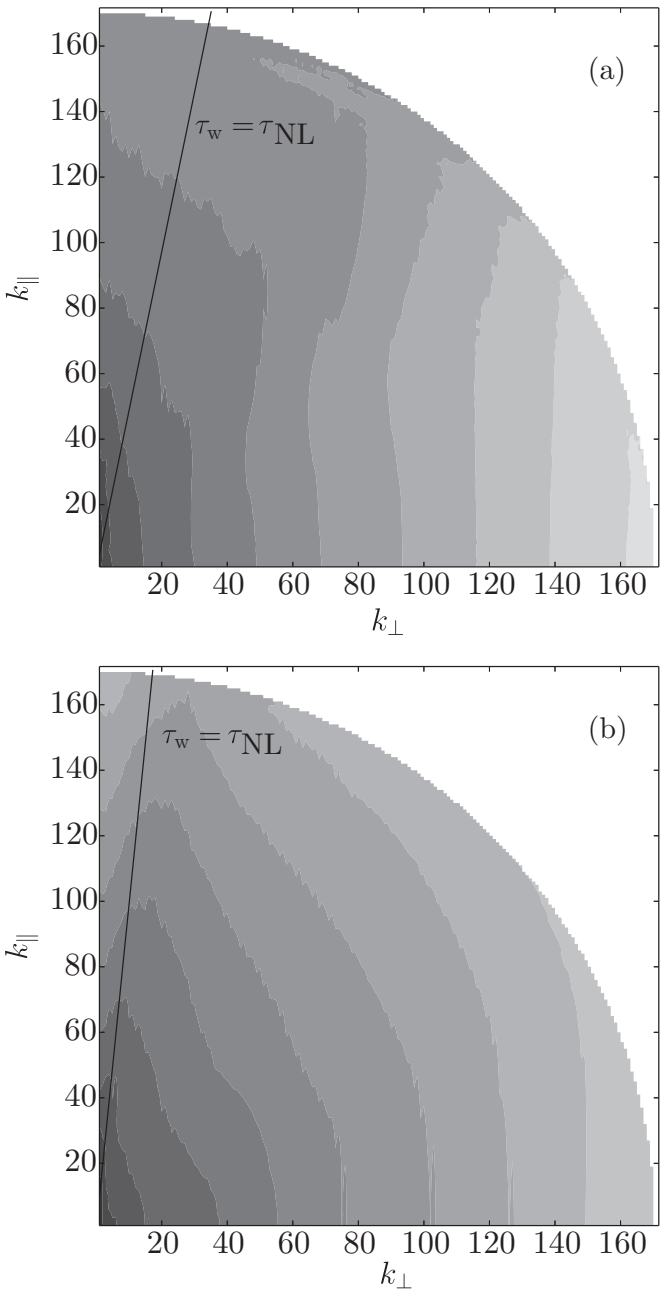

FIG. 2. Space-resolved axisymmetric energy spectrum $e(k_\perp,k_\parallel)$ for two runs with (a) Fr ≈ 0.02 and (b) Fr ≈ 0.01. Note the spectral anisotropy resulting from stratification. The solid line indicates the modes with wave period equal to the eddy turnover time, $\tau_\omega = \tau_{NL}$. In (b) a ridge is formed close to this curve, indicating energy is transferred towards modes with lower $k_\perp$ but the transfer is halted when $\tau_\omega \approx \tau_{NL}$. Modes with $\tau_\omega < \tau_{NL}$ (i.e., modes below the solid line) are often called wave modes, as these modes have the wave period as the fastest time scale. However, a proper characterization of waves requires space- and time-resolved spectra.

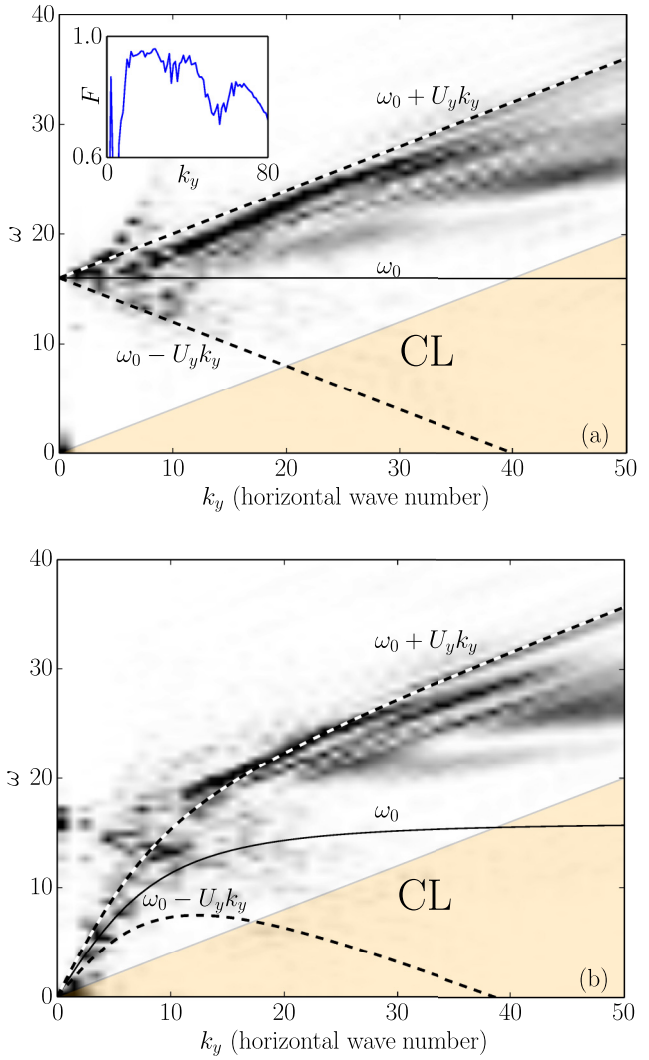

FIG. 3. (Color online) Space- and time-resolved spectrum of the potential energy $E_\theta(k_x = 0,k_y,k_z,\omega)$ (normalized by $E(\mathbf{k})$, with 0 corresponding to white and 1 corresponding to black), for Fr $= 0.01$ and for two different values of k_z: (a) $k_z = 0$ and (b) $k_z = 10$. The fundamental dispersion relation $\omega_0(\mathbf{k})$ from Eq. (3) is given by the thin solid curve, along with two Doppler-shifted branches with $U_y = \pm 0.4$ (dashed curves). Energy is mostly concentrated in the fan defined by the two shifted branches, although not uniformly distributed. Waves that travel with the flow (upper half fan) concentrate most of the power. The area shaded with light gray (transparent orange in the online version) corresponds to $\omega < U_y k_y$ with $U_y = 0.4$; note there is almost no power in this region. The defect of energy in all modes in this area indicates these waves are absorbed by critical layers (CL), with their energy being transferred to the flow. Inset: Fraction of the energy F that is contained within the two Doppler-shifted branches as a function of the wave number. In the inertial range, ≈80% of the energy corresponds to Doppler-shifted waves.

B. Spatiotemporal analysis

Precise identification of the waves, and of their role in the dynamics, requires both space and time information. Figure 3 shows different cuts of the frequency and wave-number spectrum $E_\theta(k_x,k_y,k_z,\omega)$ for $k_x = 0$ and for either $k_z = 0$ or $k_z = 10$ in the simulation with the strongest stratification and three-dimensional forcing. As internal gravity waves couple vertical motions with temperature fluctuations, we consider the spectrum of potential energy E_θ to isolate the waves more easily. In Fig. 3 there is no significant accumulation of energy in the modes that satisfy the dispersion relation given

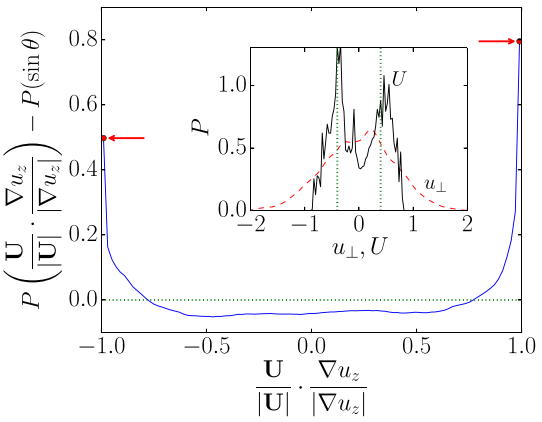

FIG. 4. (Color online) Probability density function for horizontal gradients of the vertical velocity being aligned or antialigned with the mean horizontal flow, minus the probability of having uniformly distributed alignment between the fields [θ is uniformly distributed in $[0,2\pi)$]. The PDF indicates (independently of Fig. 3) that there is an excess of waves traveling with the mean horizontal flow (compared with against the flow) and also a defect of waves propagating perpendicular to the flow. Inset: Probability distribution of the Cartesian components of the mean horizontal velocity $\mathbf{U}$ and of the pointwise horizontal velocity $\mathbf{u}_\perp$. The dotted vertical lines indicate the values ± 0.4, used to draw the Doppler-shifted branches in Fig. 3.

by Eq. (3), i.e., in modes that could be directly associated with internal gravity waves. Instead, most of the energy ($\approx$80% for $k_y \in [10,80]$) falls inside a wider region defined by the Doppler-shifted Eq. (5) with $-0.4 \leqslant U_y \leqslant 0.4$ (as a comparison, the space- and time-resolved spectrum for a simulation without Doppler shift is shown in the Appendix). The spread of the energy in this wide region suggests the waves are propagating through layers with nonzero mean horizontal velocity (i.e., VSHW). Indeed, a probability density function (PDF) of the Cartesian components of the horizontally averaged horizontal velocity $\mathbf{U}$ obtained directly from the same simulation shows two peaks at $\approx \pm 0.4$ (see the inset in Fig. 4). Also, the PDF of the pointwise horizontal velocity in the entire box is approximately Gaussian with variance close to 0.4.

It is important to remind that we force the fluid from rest at the large scales; this generates the winds, and by nonlinear interactions energy cascades towards the smaller scales. Then the cycle completes itself when the small-scale waves interact with the large-scale winds; we are not imposing flows at different scales, or imposing a background flow, as sometimes done to study interaction of waves with shear flows. Instead, we just let turbulent interactions develop by themselves. In similar simulations of turbulent stratified flows, waves have been directly observed before by measuring the frequency spectrum $E(\omega)$ or by measuring $E(\omega)$ for a few Fourier modes [26]. This study identified peaks at the frequency of the internal gravity waves, but from the frequency spectrum a relation between frequency ω and wave number $\mathbf{k}$ cannot be obtained without assuming the system is dominated by the waves (and then the relation of these quantities is given by the dispersion relation) or dominated by vortical motions (and then the relation is given by sweeping, see, e.g., Ref. [51]).

Figure 3 gives direct evidence that most of the energy is in waves. And the waves satisfy Eq. (5) where $\mathbf{U}$ is the horizontal wind. However, there is more power in modes close to the curve $\omega_0 + U_y k_y$ (with $U_y = 0.4$) than in modes close to $\omega_0 - U_y k_y$. This energy distribution cannot be explained by a preferential direction in $\mathbf{U}$ (see the PDFs in the inset in Fig. 4), by viscous effects (which introduce damping but no frequency shift), or by nonlinear corrections to the dispersion relation, as internal gravity waves are exact nonlinear solutions of the Boussinesq equations [39]. The preferential concentration is instead compatible with CL absorption. In Fig. 3 we show as a reference the area (shaded in light gray, or transparent orange in the online version), where $\omega < U_y k_y$ with $U_y = 0.4$. As in this simulation $-0.4 \lesssim U_y \lesssim 0.4$ (once again, see the PDFs in the inset in Fig. 4), for all modes in that area there is some layer with U_y such that the layer can be a CL. When the waves approach these layers, $c \approx U$, and from Eq. (7) their vertical velocity starts fluctuating more rapidly and undergo absorption in the CL transferring a fraction of their energy to the flow [13,21]. Indeed, there is almost no energy in the wave modes in this area. This indicates that CLs can be the reason for the nonlocal formation of large-scale structures in stratified turbulence observed in Refs. [30–32].

The CL mechanism can only act if $\mathrm{Ri}^{\mathrm{BF}} > 1/4$. We explicitly verified that the pointwise value of $\mathrm{Ri}^{\mathrm{BF}}$ in the simulations is larger than 1/4. As an example, for the run with $\mathrm{Fr} \approx 0.04$, the minimum of $\mathrm{Ri}^{\mathrm{BF}}$ is ≈ 14, while the simulations with lower Fr have even higher values of $\mathrm{Ri}^{\mathrm{BF}}$. Although the minimum value of this Richardson number may seem rather large when compared with atmospheric flows, it should be noted that for the sake of comparison with previous studies of CLs [11,12], the definition of $\mathrm{Ri}^{\mathrm{BF}}$ used here is based on the horizontal component of the mean large-scale flow $\mathbf{U}$ [see Eq. (6)]. In studies of stratified turbulence, the Richardson number is often defined instead using either the local vertical fluctuations of the total velocity, $\mathrm{Ri} = N^2/(\partial_z u_\perp)^2$, or local vertical fluctuations of the velocity and of the temperature, $\mathrm{Ri}^\theta = N(N - \partial_z\theta)/(\partial_z u_\perp)^2$ (where $u_\perp$ is the total perpendicular velocity field). The latter definition can be negative when vertical temperature gradients become large enough, indicating the flow can locally overturn. With these definitions, the simulation with the strongest stratification and $\mathrm{Fr} \approx 0.01$ has minimum values of $\mathrm{Ri} \approx 1$ and of $\mathrm{Ri}^\theta \approx 1$. The minimum of Ri decreases as Fr is increased (it is $\approx$0.01 in the simulation with $\mathrm{Fr} \approx 0.04$), while the minimum of Ri^θ becomes negative already in the simulation with $\mathrm{Fr} \approx 0.02$.

Internal gravity waves in a stratified fluid couple the temperature with the vertical component of the velocity. We now show that the four-dimensional power spectrum of the vertical velocity displays the same features as the spectrum of the potential energy shown above. Figure 5 shows a cut of the power spectrum of the vertical velocity $E_z(k_x = 0, k_y, k_z = 0, \omega)$ in the simulation with stronger stratification and three-dimensional forcing. The same features found in the four-dimensional spectrum of the potential energy can be found in this figure, including the Doppler shift and the defect of energy in the modes that have frequency compatible with CL absorption. In fact, the spectra are practically indistinguishable. As in the case of the temperature, a large fraction of the energy in vertical motions is also associated with

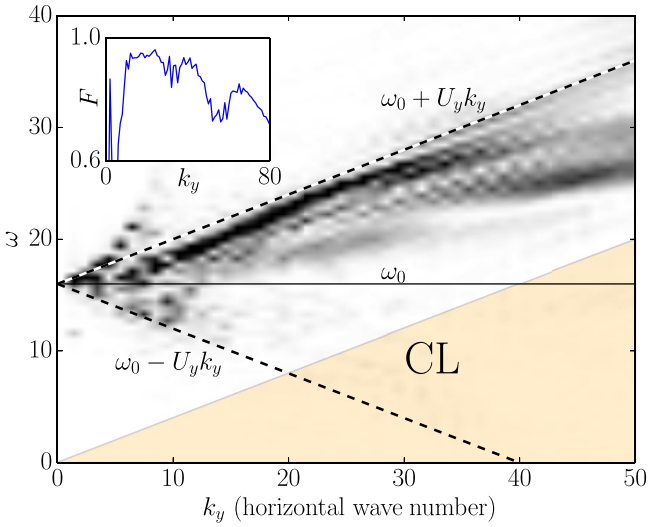

FIG. 5. (Color online) Space- and time-resolved spectrum of vertical kinetic energy $E_z(k_x = 0, k_y, k_z = 10, \omega)$, normalized by $E_z(\mathbf{k})$, and for Fr = 0.01. There is no discernible difference with the space and time spectrum of the potential temperature (see Fig. 3). The solid line corresponds to the linear dispersion relation of gravity waves, while the dashed lines indicate the two Doppler-shifted dispersion relations with $U_y = \pm 0.4$. The region shaded with light gray (transparent orange in the online version) indicates that modes that can have a CL absorption; note the lack of energy in that region. Inset: Fraction of the energy F that is contained within the two Doppler-shifted branches as a function of the wave number.

wave motions (≈80% of the energy between $10 < k_y < 80$ is inside the fan corresponding to Doppler-shifted waves, see the inset in Fig. 5). When the spectrum of horizontal velocity is considered instead, none of these signatures can be found (not shown).

As a final and independent verification of the excess of waves traveling with the flow observed in Fig. 3, we resort to a statistical analysis. As most of the energy in the simulation with Fr ≈ 0.01 is in the waves, we can assume the vertical velocity is a superposition of traveling waves $\propto e^{i(\mathbf{k}\cdot\mathbf{x}-\omega t)}$. We can then compute $\mathbf{U}\cdot\nabla u_z/(|\mathbf{U}||\nabla u_z|)$, which gives an estimation of how the wave vector (i.e., the propagation direction for a pure planar wave) is aligned with the horizontal flow. Figure 4 shows the PDF of this alignment (averaged over every layer in the fluid) minus the PDF of the sine of a uniformly distributed angle $\theta \in [0, 2\pi)$ (i.e., of randomly aligned fields with no privileged direction) for the simulation with stronger stratification and three-dimensional forcing. The result indicates a preference towards an alignment of horizontal gradients of the vertical velocity with the mean flow, as there is an excess for +1 when compared with −1 and a deficit (compared with uniformly distributed angles) for the case in which the two fields are perpendicular. Interestingly, a preference of stratified flows towards developing one sign of velocity gradients (resulting in non-Gaussian PDFs) was reported before in Ref. [52].

An interesting fact that sheds more light on how these mechanisms work is that these effects are not observed in purely rotating flows [29,51]. While these flows can also generate strong horizontal velocity fields, waves tend to travel in the vertical direction (as compared to the stratified case, where they tend to travel horizontally), and no Doppler shift develops as the waves are perpendicular to the large-scale flow.

C. Dependence on level of stratification and forcing

The results discussed so far correspond to the simulation with randomly generated three-dimensional forcing and Fr ≈ 0.01. A similar distribution of energy in frequency and wave number is observed in the simulations with same forcing but with higher Fr (i.e., weaker stratification), although the excess of waves traveling with the flow (as well as the defect in the

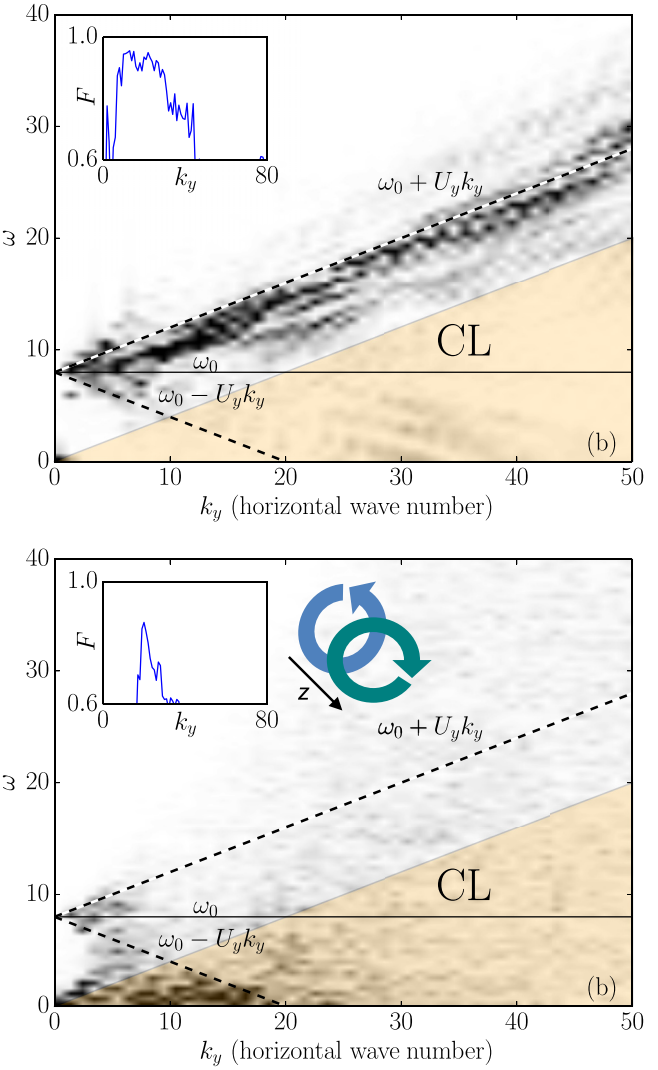

FIG. 6. (Color online) Space- and time-resolved spectrum of the potential energy $E_\theta(k_x = 0, k_y, k_z = 10, \omega)$ [normalized by $E_\theta(\mathbf{k})$] for Fr = 0.02 and for two different forcing functions: (a) three-dimensional forcing and (b) Taylor-Green forcing. Labels are as in Fig. 5. The insets show in each case the fraction of the energy F that is contained within the two Doppler-shifted branches. In (b), the inset on the right also shows a schematic representation of the Taylor-Green forcing. In (a), note the decrease in the level of stratification of the system still preserves the main features of the spectrum. In (b), the Taylor-Green forcing injects most of the energy in vortical modes ($\omega \approx 0$), the energy in the waves is therefore smaller, and the flow geometry prevents the CL absorption from developing.

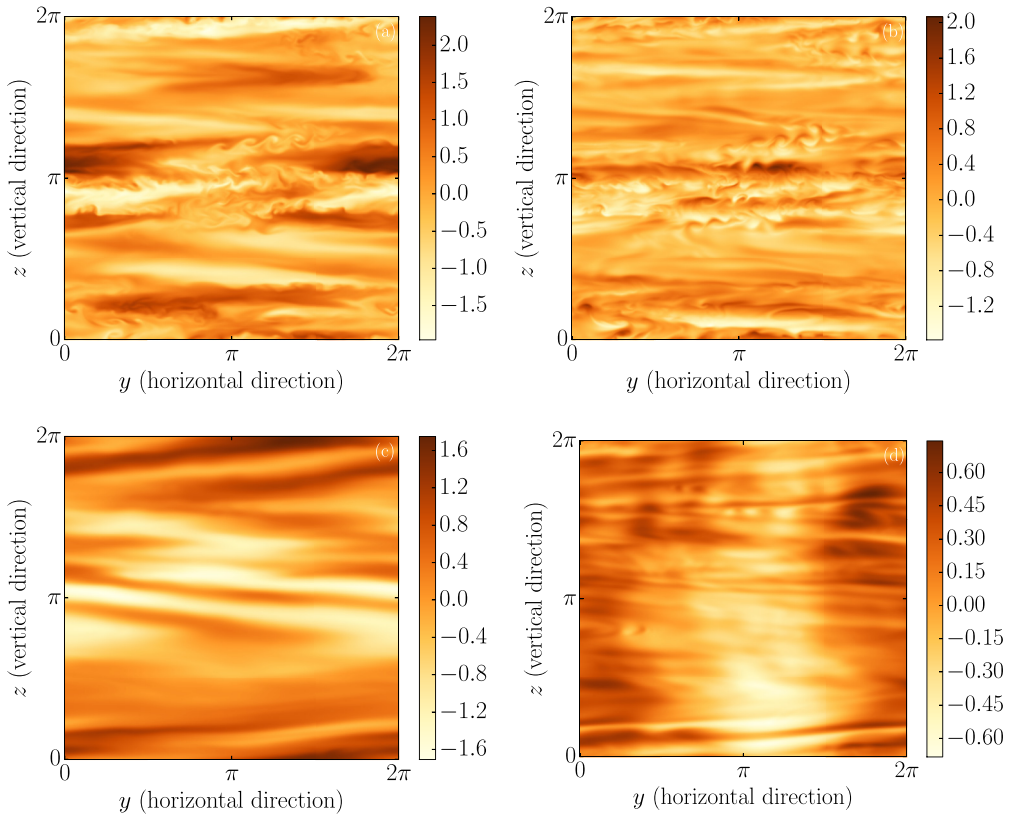

FIG. 7. (Color online) Vertical cuts (at constant $x = \pi$) of the potential temperature θ, and of the y component of the velocity field u_y, for simulations with the same Fr = 0.02 but with different forcing functions. Panels (a) and (b) correspond to Taylor-Green forcing: (a) $u_y(y,z)$ and (b) $\theta(y,z)$. Panels (c) and (d) correspond to three-dimensional forcing: (c) $u_y(y,z)$ and (d) $\theta(y,z)$. Note the more evident horizontal winds in the simulation with three-dimensional forcing, the different nature of the fluctuations in the temperature in both flows, and that, despite the overturning motions, horizontal structures and vertical shear are still present in the Taylor-Green simulation.

fan defined by the CL) is stronger in the flow with smallest Fr. Figures showing the dependence with Froude number are shown below. For Taylor-Green forcing, which prevents the formation of a mean wind in each horizontal layer, CL absorption is not observed, although Doppler spreading of the waves still takes place. These results are also presented in this section.

As a comparison with the case shown in Fig. 3, Fig. 6(a) shows the space- and time-resolved spectrum $E_\theta(k_x = 0, k_y, k_z = 0, \omega)$ for a simulation still forced with randomly generated forcing but with Fr ≈ 0.02. This spectrum can be directly compared with Fig. 3(a). Decreasing the stratification results in a spectrum that bears great resemblance with the spectrum for Fr ≈ 0.01, with nonuniform Doppler spreading of the waves and the excess of waves with $\omega \approx \omega_0 + U_y k_y$. The defect of energy in the modes compatible with CL absorption is also visible in this simulation, although the damping of these modes is slightly weaker than in the case with stronger stratification. This is compatible with the smaller fraction of energy in the waves as stratification is decreased; see the inset of Fig. 6(a). Also, this is compatible with the fact that as stratification is decreased, the power in the large-scale motions (small wave numbers) also decreases (see Fig. 1). These trends are further confirmed by the simulation with weaker stratification and Fr ≈ 0.04.

When Taylor-Green forcing is used instead, the broadening of the dispersion relation by Doppler shift can still be observed, as the energy is not concentrated along the dispersion relation but within a fan centered around it; see Fig. 6(b) for Fr ≈ 0.02, especially for wave numbers $0 < k_y \lesssim 10$. However, this effect is dimmed by a large concentration of energy in modes with $\omega \approx 0$. This is to be expected as the Taylor-Green forcing, given by $\mathbf{F} = f_0(\sin x \cos y \cos z\, \hat{x} - \cos x \sin y \cos \hat{z})$, consists of two counter-rotating vortices in the horizontal velocity and excites no vertical motions directly [see a schematic diagram in the inset of Fig. 6(b)]. As a result, the fraction of energy in wave modes is much smaller than in the case with three-dimensional forcing [see also a direct measurement of this in the inset of Fig. 6(b)]. Moreover, the imposition of the Taylor-Green vortices in each layer by the external forcing seems to disrupt the development of a nonzero mean wind in each horizontal layer, weakening also the development of CLs. Indeed, the damping of the energy in modes consistent with CL absorption in the four-dimensional spectrum of potential energy in Fig. 6(b) is almost nonexistent. As a further comparison, the space- and time-resolved spectrum for a simulation without Doppler shift and without CL absorption is shown in the Appendix.

To ease with the understanding of the behavior caused by the two different forcings, and to illustrate the presence of VSHW

in the flows, in Fig. 7 we present vertical slices (at constant $x = \pi$) of the potential temperature and horizontal velocity fields for the two simulations. Although the simulations have the same Fr and Re, the flows significantly differ. On the one hand, there are smaller-scale structures and overturning in both fields for the Taylor-Green forced simulation (this further inhibits the creation of layers that can act as CL). On the other hand, the simulation with three-dimensional forcing shows a more dominant large-scale horizontal flow and smaller-scale (although smoother) fluctuations in the temperature. This is consistent with the fact that when forcing isotropically there is more energy in the waves, as seen in Fig. 6. Another way to quantify how much energy is in the VSHW is to compare the ratio of the energy in the modes with $\omega = 0$ (i.e., in the modes with $k_\perp = 0$) to the total energy. For $\mathrm{Fr} = 0.02$, the Taylor-Green simulation has $\approx 0.009\%$ of its total energy in those modes, while the isotropically forced one has $\approx 0.03\%$, indicating that the simulation with three-dimensional forcing has stronger VSHW. Note, however, that both simulations have a broad energy spectrum, indicating that turbulence in both flows may be of different nature, with the case with more energy in wave motions being smoother and possibly closer to a wave turbulence regime.

The comparison between the two different forcing functions further indicates that stratified turbulent flows may display different behavior depending on whether the mechanism used to excite the turbulence allows or prevents the development of large-scale vertically sheared horizontal winds. Interestingly, the case studied here that injects more energy directly into the waves is also the case in which horizontal winds and CL absorption more clearly develop, two features that are not considered in wave turbulence theories.

V. CONCLUSIONS

In a turbulent flow, waves and individual absorption events cannot be easily identified. As a result, previous numerical and observational studies of Doppler shift and CL absorption focused on analyzing single wave packets traveling through a background flow. Our analysis, based on computation of a four-dimensional spectrum with high temporal and spatial resolution, allowed us to study these phenomena in turbulent flows and to identify direct evidence of their occurrence.

With these tools we showed that Doppler shift and CL absorption occur naturally in a stratified disordered flow, as a result of the interaction of the waves with the horizontal winds. This indicates CL absorption can be one of the mechanisms behind the formation of large-scale structures in stratified flows often observed in simulations but whose origin is unclear [30–32]. Moreover, although Doppler shift is observed in all forcing functions considered (except for the case discussed in the Appendix), development of CL absorption requires the external forcing not to disrupt the development of mean horizontal winds. Theories of stratified wave turbulence should take these effects into account.

The mechanism, and the tools presented here, can be also relevant in quasigeostrophic turbulence [36] and in plasma turbulence [37,38], where zonal flows are also known to develop. Moreover, CLs are known to be relevant in Rossby wave turbulence (see, e.g., Refs. [14–16]). Depending on the flow in which CLs develop, the equations that define the layer differ. As an example, while the CL in a stratified flow is given by the Taylor-Goldstein equation in Eq. (7), in the case of Rossby waves the CL follows from the Rayleigh or the Orr-Sommerfeld equation (see, e.g., Ref. [16] for a discussion of CL absorption in the context of Rossby waves and for a discussion of the shortcomings of applying wave turbulence theory in this context). In spite of these differences, the analysis presented here based on the four-dimensional spectrum should allow detection of CL absorption also in this case.

Finally, we must point out that all the results presented here were obtained with forcing functions that were kept constant in time. The differences between the forcing schemes considered indicate that results are sensitive to the way turbulence is

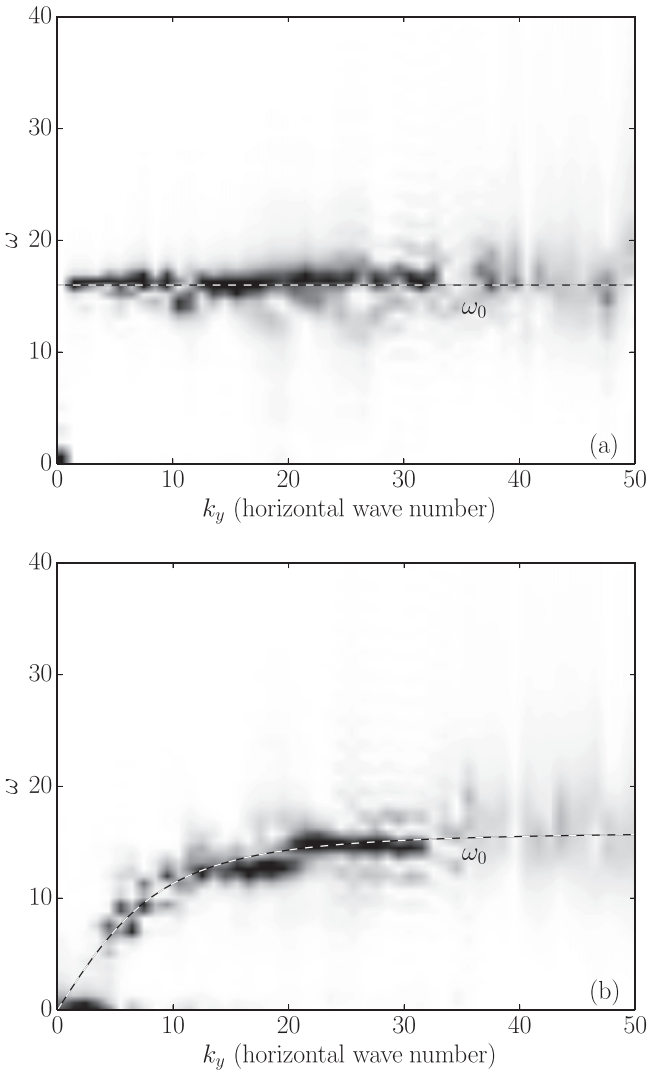

FIG. 8. Space- and time-resolved spectrum of the potential energy $E_\theta(k_x = 0, k_y, k_z, \omega)$ [normalized by $E_\theta(\mathbf{k})$] for two values of k_z: (a) $k_z = 0$ and (b) $k_z = 10$. There is no mechanical forcing in this simulation but a randomly generated, isotropic, and constant-in-time external source of temperature fluctuations. The flow is then dominated by gravity waves, with an almost negligible large-scale horizontal flow. Note the absence of CL absorption and the negligible Doppler shift; most of the energy is concentrated along the dispersion relation for the waves.

excited, but a systematic study of varying the forcing functions is beyond the objectives of this work. Using forcings that are independent of time allow for a simple isolation of the effect of the forcing (in all the four-dimensional spectra, the forcing can be identified as the energy peak near the origin, with zero frequency). As a result, the features associated with Doppler effect and CL absorption in the four-dimensional spectra could also be identified and isolated. Simulations of stratified turbulence are often performed with delta-correlated in time forcing, or with forcing at intermediate scales. A study of their effects is important and left for future work.

ACKNOWLEDGMENTS

The authors acknowledge support from Grants No. PIP 11220090100825, No. UBACYT 20020110200359, No. PICT 2011-1529, and No. PICT 2011-1626. P.C.d.L acknowledges useful comments from the organizers and attendants of the ICTP Hands-On Research School.

APPENDIX: A CASE DOMINATED BY GRAVITY WAVES

In this Appendix we present as a reference results for simulations dominated by waves and with negligible horizontal flow. As a result, the space- and time-resolved spectrum shows no signature of CL absorption, and spreading of the dispersion relation by Doppler shift is also negligible. The spectrum can then be directly compared with those presented in Figs. 3, 5, and 6 to readily identify the effect of Doppler shift and of a CL in the spectra $E_\theta(k,\omega)$ and $E_z(k,\omega)$.

To obtain simulations dominated by gravity waves, we apply no external mechanical forcing in the system [i.e., $\mathbf{F} = 0$ in Eq. (1)], and instead we force using a thermal source. In other words, Eq. (2) is replaced by

$$\partial_t\theta + \mathbf{u}\cdot\boldsymbol{\nabla}\theta = Nu_z + \kappa\nabla^2\theta + \phi, \tag{A1}$$

where ϕ is the source of temperature fluctuations. To keep the configuration of the simulation as close as possible to the simulations in the main body of the paper, ϕ is isotropic, kept constant in time, and with phases randomly generated at $t = 0$ for all Fourier modes with wave numbers between $k = 1$ and 3. All other parameters (ν, κ, and N) are kept the same as in the simulations with three-dimensional and TG mechanical forcing. The system is evolved from a fluid at rest, and once it reaches a turbulent steady state the fields are stored with high temporal cadency to compute the space- and time-resolved spectrum.

As the source of temperature fluctuations has dependence on the three spatial coordinates, horizontal flows still develop but with a smaller amplitude than in the mechanically forced case. Indeed, unlike the simulations in the main body of the text, in the steady state the r.m.s. velocity in these simulations is $u_{\rm rms} \approx 0.1$ (with horizontal velocities of the same order), while temperature fluctuations are still of order unity.

Figure 8 shows the space- and time-resolved potential energy spectrum $E_\theta(k_x = 0,k_y,k_z,\omega)$ for the simulation with stronger stratification (i.e., larger Brunt-Väisälä frequency, equal in value to the one in the mechanically forced simulation in Fig. 3). As a reference, the dispersion relation unmodified by Doppler shift given by Eq. (3) is also shown. In contrast with the spectrum in Figs. 3 and 6, the energy is mainly concentrated along this dispersion relation. This provides a direct confirmation that the simulation is indeed dominated by gravity waves. Moreover, the lack of a shift or spreading of the dispersion relation indicates Doppler shift is negligible, while the lack of a clear region with negligible wave energy indicates the absence of CL absorption.

[1] R. H. Kraichnan and D. Montgomery, Rep. Prog. Phys. **43**, 547 (1980).
[2] C. O. Hines, Nature **239**, 73 (1972).
[3] J. R. Ledwell, E. T. Montgomery, K. L. Polzin, L. C. S. Laurent, R. W. Schmitt, and J. M. Toole, Nature **403**, 179 (2000).
[4] A. Gargett, J. Wells, A. E. Tejada-Martínez, and C. E. Grosch, Science **306**, 1925 (2004).
[5] J. J. Riley and M.-P. Lelong, Annu. Rev. Fluid Mech. **32**, 613 (2000).
[6] C. Staquet and J. Sommeria, Annu. Rev. Fluid Mech. **34**, 559 (2002).
[7] G. Ivey, K. Winters, and J. Koseff, Annu. Rev. Fluid Mech. **40**, 169 (2008).
[8] J. J. Finnigan, F. Einaudi, and D. Fua, J. Atmos. Sci. **41**, 2409 (1984).
[9] K. Dohan and B. R. Sutherland, Phys. Fluids **15**, 488 (2003).
[10] J. Xing and A. M. Davies, J. Geophys. Res. **110**, C05003 (2005).
[11] R. Grimshaw, J. Fluid Mech. **54**, 193 (1972).
[12] R. Grimshaw, J. Atmos. Sci. **32**, 1779 (1975).
[13] C. O. Hines, J. Atmos. Sci. **48**, 1361 (1991).
[14] P. D. Killworth and M. E. McIntyre, J. Fluid Mech. **161**, 449 (1985).
[15] P. H. Haynes, J. Fluid Mech. **161**, 493 (1985).
[16] E. S. Benilov, V. G. Gnevyshev, and V. I. Shrira, Dyn. Atmos. Oceans **16**, 339 (1992).
[17] E. E. Gossard, J. H. Richter, and D. Atlas, J. Geophys. Res. **75**, 3523 (1970).
[18] E. Kunze, A. J. Williams, and M. G. Briscoe, J. Geophys. Res. Oceans **95**, 18127 (1990).
[19] S. A. Thorpe, J. Fluid Mech. **103**, 321 (1981).
[20] C. G. Koop and B. McGee, J. Fluid Mech. **172**, 453 (1986).
[21] K. B. Winters and E. A. D'Asaro, J. Fluid Mech. **272**, 255 (1994).
[22] D. Broutman, C. Macaskill, M. E. McIntyre, and J. W. Rottman, Geophys. Res. Lett. **24**, 2813 (1997).
[23] P. Billant and J.-M. Chomaz, Phys. Fluids **13**, 1645 (2001).
[24] M. L. Waite and P. Bartello, J. Fluid Mech. **546**, 313 (2006).
[25] G. Brethouwer, P. Billant, E. Lindborg, and J.-M. Chomaz, J. Fluid Mech. **585**, 343 (2007).
[26] E. Lindborg and G. Brethouwer, J. Fluid Mech. **586**, 83 (2007).
[27] P. Bartello, J. Atmos. Sci. **52**, 4410 (1995).
[28] A. Pouquet and R. Marino, Phys. Rev. Lett. **111**, 234501 (2013).
[29] E. Yarom and E. Sharon, Nat. Phys. **10**, 510 (2014).

[30] L. M. Smith and F. Waleffe, J. Fluid Mech. **451**, 145 (2002).
[31] R. Marino, P. D. Mininni, D. Rosenberg, and A. Pouquet, Europhys. Lett. **102**, 44006 (2013).
[32] R. Marino, P. D. Mininni, D. L. Rosenberg, and A. Pouquet, Phys. Rev. E **90**, 023018 (2014).
[33] C. Herbert, A. Pouquet, and R. Marino, J. Fluid Mech. **758**, 374 (2014).
[34] S. Nazarenko, *Wave Turbulence*, 1st ed. (Springer, Berlin, 2011).
[35] Y. V. Lvov and E. G. Tabak, Phys. Rev. Lett. **87**, 168501 (2001).
[36] I. N. James, J. Atmos. Sci. **44**, 3710 (1987).
[37] P. H. Diamond, S.-I. Itoh, K. Itoh, and T. S. Hahm, Plasma Phys. Contr. F. **47**, R35 (2005).
[38] C. Connaughton, S. Nazarenko, and B. Quinn, Europhys. Lett. **96**, 25001 (2011).
[39] A. Majda, *Introduction to PDEs and Waves for the Atmosphere and Ocean* (American Mathematical Society, New York, 2003).
[40] J. R. Booker and F. P. Bretherton, J. Fluid Mech. **27**, 513 (1967).
[41] D. C. Fritts and M. A. Geller, J. Atmos. Sci. **33**, 2276 (1976).
[42] N. Smyth, J. Austral. Math. Soc. Ser. B **29**, 352 (1988).
[43] S. N. Brown and K. Stewartson, J. Fluid Mech. **100**, 577 (1980).
[44] S. N. Brown and K. Stewartson, J. Fluid Mech. **115**, 217 (1982).
[45] S. N. Brown and K. Stewartson, J. Fluid Mech. **115**, 231 (1982).
[46] D. O. Gómez, P. D. Mininni, and P. Dmitruk, Adv. Space Res. **35**, 899 (2005).
[47] D. O. Gómez, P. D. Mininni, and P. Dmitruk, Phys. Scripta **2005**, 123 (2005).
[48] P. Mininni, D. Rosenberg, R. Reddy, and A. Pouquet, Parallel Comput. **37**, 316 (2011).
[49] J. J. Riley and S. M. deBruynKops, Phys. Fluids **15**, 2047 (2003).
[50] J. Schumacher, J. D. Scheel, D. Krasnov, D. A. Donzis, V. Yakhot, and K. R. Sreenivasan, Proc. Natl. Acad. Sci. USA **111**, 10961 (2014).
[51] P. Clark di Leoni, P. J. Cobelli, P. D. Mininni, P. Dmitruk, and W. H. Matthaeus, Phys. Fluids **26**, 035106 (2014).
[52] C. Rorai, D. Rosenberg, A. Pouquet, and P. D. Mininni, Phys. Rev. E **87**, 063007 (2013).